Optical properties of functionalized graphene

J. L. Cheng, C. Salazar, and J. E. Sipe
Department of Physics and Institute for Optical Sciences, University of Toronto, 60 St. George Street, Toronto, Ontario, Canada M5S 1A7
(Received 27 May 2013; published 29 July 2013)

We use *ab initio* calculations to investigate the geometry, band structures, and optical properties of hydrogen functionalized graphene, where hydrogen atoms are attached periodically to A-site carbon atoms to form $\sqrt{3} \times \sqrt{3}$, 2×2, 3×3, 4×4, and 5×5 supercells. The adsorbed hydrogen atoms distort the carbon atoms vertically, with almost no modification of the in-plane structures. The ground states show ferromagnetic order, with a total energy of a few tens meV lower than the nonmagnetic ground state. The hydrogen adsorption opens a gap that depends on the supercell size. Optical conductivities are calculated and show fine structures at the band edge. Taking into account the spin-orbit coupling, the nonzero off-diagonal components of the conductivity predict Kerr and Faraday effects without an external magnetic field.

DOI: 10.1103/PhysRevB.88.045438 PACS number(s): 73.22.Pr, 78.67.Wj, 61.48.Gh

I. INTRODUCTION

Due to its high transport mobility, long spin relaxation time, and low optical absorption, graphene has become a popular and important material for studies in electronics, spintronics, and photonics, as well as their integrated fields.[1–3] Most of the potential applications stem from graphene's peculiar linear dispersion relation, a direct result of which is a universal optical conductivity[4] $\sigma_0 = e^2/4\hbar$ that survives over a wide energy range. However, the nonzero dc limit of conductivity makes graphene unsuitable for applications in standard digital electronic circuitry where a high on/off ratio is required. One way to open a gap is to functionalize graphene in order to break π bonds by adsorbing hydrogen atoms,[5] diazonium groups,[6] or aryl groups[7,8] that are in many ways functionally identical to hydrogen adatoms. These adsorbates can form periodic patterns;[6,9] for example, a 2×2 supercell has been observed experimentally following diazonium functionalization

Functionalization changes graphene properties dramatically in many respects.[10–12] First is the geometry and band structure. Theoretically, hydrogenated graphene has been studied in the most detail,[13–19] and some of the changes are understood. Generally, hydrogen atoms distort the local geometry of graphene by locally rehybridizing the bonding[20] from $p_z + sp^2$ to sp^3, and the potential of the H^+ ionic core causes the gap to open. Fully hydrogenated graphene (graphane) has a predicted LDA gap of 3.4 eV[21] and a GW^0 gap of 5.0 eV. The stable half-hydrogenated graphene (graphone) acquires a stable structure by attaching hydrogen on both sides alternatively, which gives an LDA gap of 3.5 eV.[19] Choi[14] investigated the band structure of hydrogenated graphene with different hydrogen coverage, and found the band gap satisfies the "1/3 rule"[22] and is proportional to the square root of the hydrogen coverage. Some of these structures have been synthesized and measured.[5,23,24]

Functionalization can play an important role in transport properties[25,26] and spintronics.[27] With orbital rehybridization, the spin-orbit coupling can be enhanced by orders of magnitude around the Dirac points,[27] which may be the reason for the unexpected spin relaxation rates observed in experiments. For structures where functionalization only appears on one carbon site of graphene, an important result is the appearance of a spin-polarized gap,[20] and the localization of magnetism on the other carbon site with an unpaired electron. Unlike most magnetic materials, the magnetism in functionalized graphene involves the $2p$ orbital, and it has been suggested that it could be important for applications in spintronics. Yazyov *et al.*[10,28,29] investigated these magnetic properties with both *ab initio* calculations and a Hubbard model.

In this paper, we consider the ferromagnetic ground states of hydrogen-functionalized graphene. After reinvestigating the band structures of supercells with different hydrogen coverage, we calculate optical conductivities, which show an enhancement and a fine structure around the band edge. We also find that for majority spins the lowest energy optical transitions are between the impurity band and the π^* band of graphene, whereas for minority spins they are between the π band of graphene and the impurity band. Furthermore, introducing the spin-orbit coupling, we find that these structures show Kerr and Faraday effects without an external magnetic field. This response could be taken as one of the signatures of ferromagnetic ground states.

Our paper is organized as follows: We introduce our model and some numerical details in Sec. II, and then present the calculated band structures for different supercells in Sec. III. With wave functions from *ab initio* calculations and the associated velocity matrix elements, we calculate the diagonal components of the optical conductivity tensor, ignoring the spin-orbit coupling, in Sec. IV. Then we treat the spin-orbit coupling perturbatively and calculate the off-diagonal terms of the optical conductivity tensor in Sec. V. Our conclusions are given in Sec. VI.

II. MODEL AND CALCULATION METHOD

We model functionalized graphene as a supercell formed by $n \times n$ graphene unit cells in which one hydrogen atom is chemisorbed on top of one A-site carbon atom [denoted as A_0; see Fig. 1(c)], with a hydrogen coverage of $1/n^2$. In our calculations, n is taken as $\sqrt{3}$, 2, 3, 4, and 5. Illustrations of the $\sqrt{3} \times \sqrt{3}$ and 2×2 supercells are shown from a top view in Figs. 1(a) and 1(b). The hydrogen atom distorts the graphene lattice by lifting carbon atoms at the A_0 site out of the plane and rehybridizing the $p_z + sp^2$ orbitals to sp^3 [see Fig. 1(c)]. The distortion also makes other carbon

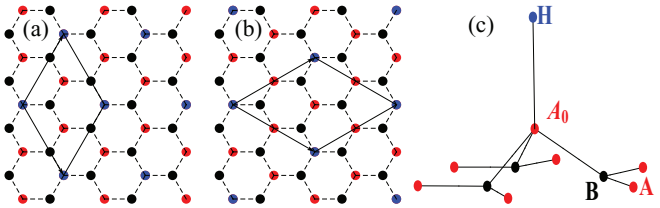

FIG. 1. (Color online) Top view of supercells of (a) $\sqrt{3} \times \sqrt{3}$ and (b) 2×2 functionalized graphene structures. Red/black dots are the A/B sites, blue dots indicate hydrogen atoms. (c) The front view of the local distortion around A_0 sites.

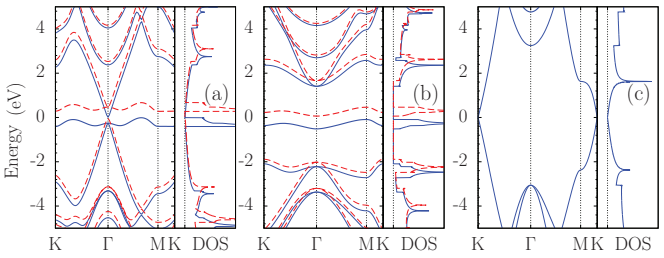

FIG. 2. (Color online) Band structures and density of states near the band gap for (a) $\sqrt{3} \times \sqrt{3}$ supercell, (b) 2×2 supercell, and (c) pristine graphene. Dashed red curves: spin-up bands; solid blue curves: spin-down bands.

atoms buckle slightly out of the graphene plane. Due to bonding between the hydrogen atom and the A_0 carbon atom, there exists one unpaired electron on the B-site carbon atom, which can lead to the nonzero magnetism.[20] Both *ab initio* and Hubbard model[10,28,29] calculations have shown that the ground states of these structures have magnetic ordering. Supercells for magnetic ground states do not coincide with the geometric supercell in general, except in the ferromagnetic phase. For simplicity, we only consider the ferromagnetic and nonmagnetic ground states here.

The optimum geometries and ground states are determined from density-functional theory (DFT) calculations using the freely available ABINIT code,[30] where the local-density approximation to the exchange-correlation density functional is used; we employ Troullier-Martins pseudopotentials. In our DFT calculations, we checked that the spin-orbit coupling leads to minor corrections to the ground state; we treat it perturbatively later. We take the energy cutoff as 30 hartrees and the length of the supercell along the z direction as 20 bohrs. In our structure optimizations, the in-plane position of each atom is fixed, and the z components are relaxed using the Broyden-Fletcher-Goldfarb-Shanno minimization method. The unit cell information, the parameters used in the calculation, and the results are listed in Table I.

In the structure optimization, our calculations are performed for both ferromagnetic and nonmagnetic ground states, which give the same results: The carbon-hydrogen bond length is about 1.14 Å for all cases, and the A_0 site carbon atom is lifted out of the graphene plane by about 0.35 Å in the z direction, which is associated with the rehybridization towards sp^3 orbitals. The stability of the ground states can be identified by the adsorption energy, which is defined as

$$E_{\text{ads}} = -E_{\text{tot}}(\text{graphene} + \text{H}) + E_{\text{tot}}(\text{graphene}) + E_{\text{tot}}(\text{H}). \tag{1}$$

Both calculations give similar E_{ads}, which is about 0.8–1 eV for all structures, but the ferromagnetic ground state has a lower energy by about 50–170 meV.

III. BAND STRUCTURES

LDA calculations show that all structures have nonzero band gaps for both majority and minority spin branches. Table I lists the band gap for each spin branch. Because DFT calculations usually underestimate the band gap, the real band gap in functionalized graphene may be larger, and GW calculations are necessary to take into account many-body effects. Band structures and densities of states (DOS) are plotted for $\sqrt{3} \times \sqrt{3}$ and 2×2 supercells in Fig. 2 and for 3×3, 4×4, and 5×5 supercells in Fig. 3. The effect of adsorbing a hydrogen atom is obvious: (i) Considering the

TABLE I. Parameters used in the geometry optimization and part of the results. Here $\boldsymbol{a}'_1 = \frac{a_0}{2}(\sqrt{3}, -1)$ and $\boldsymbol{a}'_2 = \frac{a_0}{2}(\sqrt{3}, 1)$ are the primitive lattice vectors of graphene, with the experimental value $a_0 = 4.6487$ bohrs, $\boldsymbol{b}'_i = \frac{2\pi}{a_0}(\frac{1}{\sqrt{3}}, -1)$ and $\boldsymbol{b}'_2 = \frac{2\pi}{a_0}(\frac{1}{\sqrt{3}}, -1)$ are the reciprocal primitive vectors of graphene, $\boldsymbol{a}_i$ and $\boldsymbol{b}_i$ are the corresponding quantities in functionalized graphene, z_H is the C-H bond length, and $-z_B$ is the lifting of A_0 carbon atoms; E_{ads} ($E_{\text{ads}} + \delta E_{\text{ads}}$) is the adsorption energy of the ferromagnetic/nonmagnetic ground states; and E_g is the direct gap for majority and minority spin branches, respectively.

	$\sqrt{3} \times \sqrt{3}$	3×3	3×6	2×2	4×4	5×5
$\boldsymbol{a}_1$	$2\boldsymbol{a}'_1 - \boldsymbol{a}'_2$	$3\boldsymbol{a}'_1$	$6\boldsymbol{a}'_1$	$2\boldsymbol{a}'_1$	$4\boldsymbol{a}'_1$	$5\boldsymbol{a}'_1$
$\boldsymbol{a}_2$	$-\boldsymbol{a}'_1 + 2\boldsymbol{a}'_2$	$3\boldsymbol{a}'_2$	$3\boldsymbol{a}'_2$	$2\boldsymbol{a}'_2$	$4\boldsymbol{a}'_2$	$5\boldsymbol{a}'_2$
$\boldsymbol{b}_1$	$\frac{2}{3}\boldsymbol{b}'_1 + \frac{1}{3}\boldsymbol{b}'_2$	$\frac{1}{3}\boldsymbol{b}'_1$	$\frac{1}{6}\boldsymbol{b}'_1$	$\frac{1}{2}\boldsymbol{b}'_1$	$\frac{1}{4}\boldsymbol{b}'_1$	$\frac{1}{5}\boldsymbol{b}'_1$
$\boldsymbol{b}_2$	$\frac{1}{3}\boldsymbol{b}'_1 + \frac{2}{3}\boldsymbol{b}'_2$	$\frac{1}{3}\boldsymbol{b}'_2$	$\frac{1}{5}\boldsymbol{b}'_2$	$\frac{1}{3}\boldsymbol{b}'_2$	$\frac{1}{2}\boldsymbol{b}'_2$	$\frac{1}{4}\boldsymbol{b}'_2$
$\boldsymbol{k}$ grid	$14 \times 14 \times 1$	$10 \times 10 \times 1$	$5 \times 10 \times 1$	$10 \times 10 \times 1$	$10 \times 10 \times 1$	$6 \times 6 \times 1$
z_H (Å)	1.147	1.141	1.141	1.143	1.141	1.140
z_B (Å)	−0.352	−0.356	−0.359	−0.343	−0.357	−0.357
E_{ads} (eV)	0.81	0.924	0.945	0.92	0.959	0.982
δE_{ads} (eV)	0.174	0.082	0.061	0.140	0.058	0.045
E_g (eV)	0.281,0.534	0.158,0.165	0.088,0.083	1.921,2.085	0.682,0.679	0.595,0.554

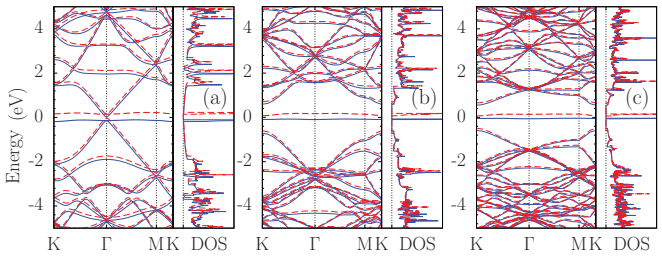

FIG. 3. (Color online) Band structures and density of states near band gap for (a) 3×3, (b) 4×4, and (c) 5×5 supercells, labeled as in Fig. 2.

ferromagnetic ground state, the majority and minority band degeneracy is broken, and insulator band structures result for both spin branches. For larger supercells, the difference between these two branches decreases. (ii) The hydrogen atom introduces two spin-dependent impurity bands located around the Fermi energy, with one filled and the other empty. For later use, we note that the band index of impurity bands is 13 for the $\sqrt{3} \times \sqrt{3}$ supercell and 17 for the 2×2 supercell. The widths of the impurity bands are narrow (<0.5 eV) and decrease with increasing supercell size, which can be clearly seen in DOS. The narrow impurity bands are the source of the magnetism in functionalized graphene. (iii) Band gaps show an interesting dependence on the supercell size, and can be divided into two classes: One class has small band gaps, and includes the $\sqrt{3} \times \sqrt{3}$ and 3×3 supercells, as well as the 3×6 supercell which was calculated for confirmation; the other has large band gaps, and includes 2×2, 4×4, and 5×5 supercells. In each class, the band gap always decreases with increasing supercell size, naturally enough because the effect of the hydrogen atom decreases with increasing supercell size. But gaps in the first class are always smaller than those in the second class. The size dependence of the band gap is similar to the "1/3 rule" found in carbon nanotubes.[22]

To understand these features better, we consider how the graphene π and π^* bands are connected to the functionalized graphene states under the effect of hydrogen adsorption. This connection originates from the Brillouin zone (BZ) folding. Each $\boldsymbol{\kappa}$ point in the BZ of functionalized graphene (blue rhombus in Fig. 4) is associated with n^2 points $\{\boldsymbol{k}_i, i = 1, \cdots, n^2\}$ in the BZ of graphene (black rhombus) that are folded to it.

Considering only the p_z orbitals, the tight-binding Hamiltonian is written as

$$H = t \sum_{\langle ij \rangle} c^\dagger_{A;i} c_{B;j} + \frac{\varepsilon_H}{2} \sum_{A_0} h^\dagger_{A_0} h_{A_0} + \Delta \sum_{A_0} h^\dagger_{A_0} c_{A_0} + \text{H.c.} \tag{2}$$

Here t is the coupling strength between the A and B carbon atoms, ε_H is the s orbital energy of the hydrogen atom, Δ is the coupling strength between the hydrogen atom and the A_0-site carbon atom. In terms of Fourier-transformed operators the Hamiltonian is written as

$$H = t \sum_{\boldsymbol{\kappa}} \sum_{j} \left[f_{\boldsymbol{k}_j} c^\dagger_{A;\boldsymbol{k}_j} c_{B;\boldsymbol{k}_j} + \text{H.c.} \right] + \varepsilon_H \sum_{\boldsymbol{\kappa}} h^\dagger_{\boldsymbol{\kappa}} h_{\boldsymbol{\kappa}} + \frac{\Delta}{n} \sum_{\boldsymbol{\kappa};j} \left[h^\dagger_{\boldsymbol{\kappa}} c_{A;\boldsymbol{k}_j} + \text{H.c.} \right] \tag{3}$$

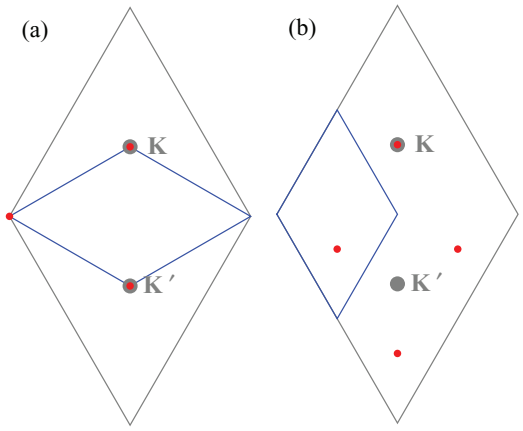

FIG. 4. (Color online) BZ fold for the $\sqrt{3} \times \sqrt{3}$ (a) and 2×2 (b) supercells. The BZ for graphene and functionalized graphene are expressed by gray and blue rhombus, respectively. The two big gray dots are Dirac points in graphene. All red points are folded into the same $\boldsymbol{\kappa} = \Gamma$ (a) or $\boldsymbol{\kappa} = K$ (b) point in the functionalized graphene BZ.

with $f_{\boldsymbol{k}} = 1 + e^{-i\boldsymbol{k}\cdot\boldsymbol{b}'_1} + e^{-i\boldsymbol{k}\cdot\boldsymbol{b}'_2}$. Focusing on the changes of the graphene states at the Dirac points, we have the following: (i) The coupling strength Δ/n implies that the gap has square root dependence of the hydrogen coverage. (ii) For any n, the two states $|\psi\rangle = c^\dagger_{B;\boldsymbol{K}}|\text{vac}\rangle$ and $|\psi'\rangle = c^\dagger_{B;\boldsymbol{K}'}|\text{vac}\rangle$ are still eigenstates with zero energies. (iii) For the $\sqrt{3} \times \sqrt{3}$, 3×3, and 3×6 supercells where the "1/3 rule" is applied, both Dirac points are folded to Γ points, and the state $|\psi''\rangle = \frac{1}{\sqrt{2}}(c^\dagger_{A;\boldsymbol{K}} - c^\dagger_{A;\boldsymbol{K}'})|\text{vac}\rangle$ is another eigenstate with zero energy. Thus, in the first class, there exists a threefold degeneracy at zero energy, which results in a zero gap in this approximated model. The small gap in our calculations comes from the distortion of the sp^2 hybrid orbitals.

IV. OPTICAL RESPONSE

We have calculated the optical conductivity of these structures, where the in-plane response is given as $J^a(\omega) = \sigma^{ab}(\omega) E^b(\omega)$ with $a, b = x, y$ and

$$\sigma^{ab}(\omega) = \frac{ie^2}{\hbar} \sum_{cv\boldsymbol{k}} \left[\frac{v^a_{vc\boldsymbol{k}} v^b_{cv\boldsymbol{k}}}{\omega_{cv\boldsymbol{k}}(\omega - \omega_{cv\boldsymbol{k}} + i\delta)} - \{c \leftrightarrow v\} \right], \tag{4}$$

where $\hbar\omega_{cv\boldsymbol{k}} = \varepsilon_{c\boldsymbol{k}} - \varepsilon_{v\boldsymbol{k}}$ gives the transition energy between the conduction and valence band, with $\varepsilon_{n\boldsymbol{k}}$ being the nth band energy, and $v^a_{cv\boldsymbol{k}}$ the interband velocity matrix elements. The velocity matrix elements are interpolated from ABINIT results by using the method described in the Appendix.

To evaluate this expression numerically, we use $(\omega - \omega_{cv\boldsymbol{k}} + i\delta)^{-1} = P(\omega - \omega_{cv\boldsymbol{k}})^{-1} - i\pi\delta(\omega - \omega_{cv\boldsymbol{k}})$ and rewrite the conductivity as $\sigma^{ab}(\omega) = \sigma^{ab}_1(\omega) + i\sigma^{ab}_2(\omega)$, where $\sigma^{ab}_1(\omega)$ and $\sigma^{ab}_2(\omega)$ are real,

$$\sigma^{ab}_1(\omega) = \frac{\pi e^2}{\hbar} \sum_{cv\boldsymbol{k}} \left[v^a_{vc\boldsymbol{k}} r^b_{cv\boldsymbol{k}} \delta(\omega - \omega_{cv\boldsymbol{k}}) - \{c \leftrightarrow v\} \right], \tag{5}$$

and $\sigma^{ab}_2(\omega)$ is calculated using the Kramers-Krönig relation. We calculate $\sigma^{ab}_1(\omega)$ by the linear analytic tetrahedral

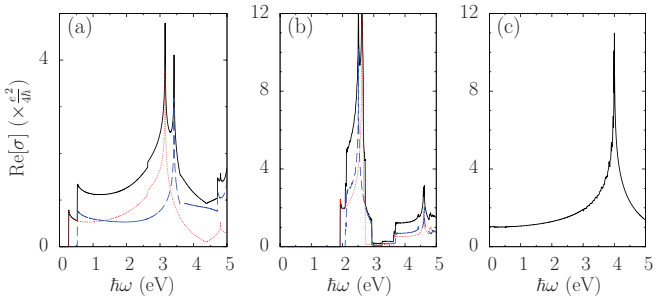

FIG. 5. (Color online) Real part of the optical conductivity for $\sqrt{3} \times \sqrt{3}$ supercell (a), 2×2 supercell (b), and pristine graphene (c). Red dotted (blue dashed) curves are the contribution from the majority (minority) spin branch; black solid curves are the total.

integration method on a homogeneous grid over the whole BZ. Without spin-orbit coupling, the system has D_3 symmetry, which gives $\sigma^{xx} = \sigma^{yy}$ and $\sigma^{xy} = \sigma^{yx} = 0$. The absorption is determined by σ_1^{xx}. In Fig. 5 we plot the real part of the optical conductivity for the $\sqrt{3} \times \sqrt{3}$ (a) and 2×2 (b) supercell, as well as pristine graphene (c) as a reference. Due to dramatic changes in the band structure at both low and high energies, the conductivity in functionalized graphene shows a behavior totally different from pristine graphene: (i) A gap appears; (ii) two spin channels give different optical conductivities and show fine structures for band edge transitions; (iii) the absorption peak induced by the Van Hove singularity around the M point in pristine graphene is redshifted in functionalized graphene; (iv) the optical conductivity is enhanced at the band edge. To understand these features, we give the band-resolved transitions between impurity bands and graphene π/π^* bands in Fig. 6. Unlike the transition in pristine graphene, which is between the π and π^* bands, here it is from the filled impurity band to the π^* band for the majority spin branch (from the π band to the empty impurity band for the minority spin branch). Due to the narrow impurity bands, the large DOS enhances the absorption around the band edge. Because the energy of the impurity bands is between π and π^* bands, the characteristic energy for the absorption peak also shifts.

The optical conductivities for the 3×3, 4×4, and 5×5 supercells are given in Fig. 7.

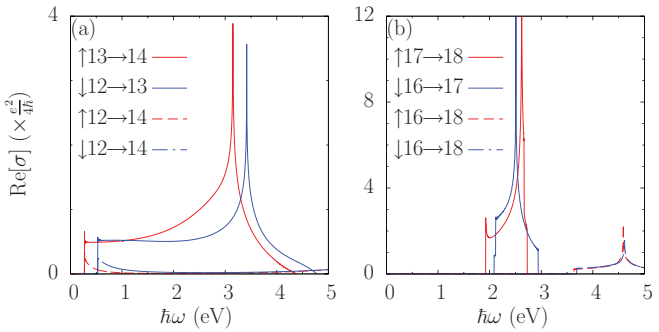

FIG. 6. (Color online) Band-resolved contribution to the optical conductivity for $\sqrt{3} \times \sqrt{3}$ (a) and 2×2 (b) supercells. The impurity bands are labeled by 13 and 17, respectively. We use ↑ (↓) to indicate the majority (minority) bands.

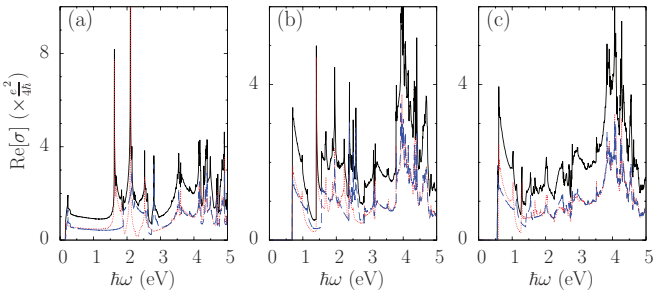

FIG. 7. (Color online) Optical conductivity for (a) 3×3, (b) 4×4, and (c) 5×5 supercells, labeled as in Fig. 5.

V. SPIN-ORBIT COUPLING

Because both carbon and hydrogen are very light elements, their spin orbit coupling is weak and can be treated perturbatively. For the hydrogen s orbital, the spin-orbit coupling can be ignored; for the carbon $2p$ orbital we take the form widely used in the empirical pseudopotential calculation[31]

$$v_{\rm so}(\boldsymbol{r}) = \lambda\theta(r - 2a_B)\hat{\boldsymbol{L}} \cdot \hat{\boldsymbol{\sigma}}\mathcal{P}_1, \tag{6}$$

where $\hat{\boldsymbol{L}}$ is the angular momentum operator and $\mathcal{P}_l$ is the projector on the orbital momentum state l. The crystal potential induced by this term is $V_{\rm so}(\boldsymbol{r}) = \sum_{\boldsymbol{R}} v_{\rm so}(\boldsymbol{r} - \boldsymbol{R})$, with $\boldsymbol{R}$ being the position of a carbon atom nucleus. The coupling parameter $\lambda = -3.78 \times 10^{-3}$ eV is fitted to the spin split energy at the Γ point of graphene, which is about 9 meV, as obtained from a spinor LDA calculation.[32] With the inclusion of the spin-orbit coupling, we rediagonalize the total Hamiltonian to obtain the new eigenstates and eigenenergies. The symmetry of the electronic states is reduced to C_3, which gives $\sigma^{xy}(\omega) = -\sigma^{yx}(\omega)$ for the off-diagonal components of the conductivity tensor; the calculated $\sigma^{xx}(\omega)$ is the same as before. In calculating $\sigma^{xy}(\omega)$, a nonzero damping of $\delta = 0.05$ eV is used to make the plot smooth. Results are given in Fig. 8 for the $\sqrt{3} \times \sqrt{3}$ and 2×2 supercells. The magnitude of the off-diagonal terms is about two orders smaller than the diagonal terms.

We turn to the possibility of experimentally detecting such a small response. The off-diagonal response $\sigma^{xy}(\omega) = -\sigma^{yx}(\omega)$ implies that Kerr and Faraday effects could in principle be

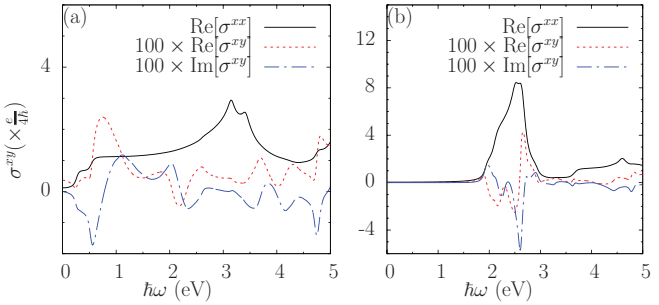

FIG. 8. (Color online) Off-diagonal components of the conductivity tensor $\sigma^{xy}(\omega)$. The real and imaginary parts are given by red dashed (blue chain) curves for (a) $\sqrt{3} \times \sqrt{3}$ and (b) 2×2 supercells. A damping of $\delta = 0.05$ eV is used in the calculation. The black curves are the real part of the diagonal component $\sigma^{xx}(\omega)$.

seen in functionalized graphene without an external magnetic field. The Kerr or Faraday rotation angle[33] for normally incident light is about $2\mathrm{Re}[\sigma^{xy}]/(n_r^2-1+2\mathrm{Re}[\sigma^{xx}])$ or $\mathrm{Re}[\sigma^{xy}]/(n_r+1)$, with n_r being the refractive index of the substrate. For functionalized graphene on a substrate, both angles are about 10^{-4} rad. In an extreme case for a freestanding functionalized graphene in air, the Kerr rotation angle can be as large as 10^{-2} rad.

VI. CONCLUSION

We use *ab initio* calculations to study the geometry, band structure, and optical response of hydrogen functionalized graphene with different supercells. Ferromagnetically electronic structures have lower energies than nonmagnetic electronic structures. In the ground states, the band structures are spin polarized with nonzero gap for both spin branches. The hydrogen atom behaves as an impurity to form two impurity bands with one filled (majority) and the other empty (minority), and breaks the degeneracy of the π and π^* bands of graphene at the Dirac points. The dominant contributions to the optical conductivity are transitions between the filled impurity band and π^* band, and between the π band and the empty impurity band, and they show enhancement and fine structure at band edge. Including the spin-orbit coupling, these structures are predicted to exhibit Kerr and Faraday effects without an external magnetic field, which could be taken as an experimental signature of the ferromagnetic ground states in functionalized graphene.

ACKNOWLEDGMENTS

This work was supported by the Natural Sciences and Engineering Research Council of Canada. C.S. acknowledges partial support from Mexico's CONACYT. We thank Theodore B. Norris and Robert C. Haddon for valuable discussions.

APPENDIX: VELOCITY MATRIX ELEMENTS FROM ABINIT

With the converged ground state, we can use ABINIT to produce the Kohn-Sham eigenstates and eigenenergies by non-self-consistent calculations. An eigen wave function $\psi_{n\boldsymbol{k}}(\boldsymbol{r})$ is expanded in a plane wave basis as $\psi_{n\boldsymbol{k}}(\boldsymbol{r}) = \frac{1}{\sqrt{V}}e^{i\boldsymbol{k}\cdot\boldsymbol{r}}\sum_{\boldsymbol{G}} C_{n\boldsymbol{k}}(\boldsymbol{G})e^{i\boldsymbol{G}\cdot\boldsymbol{r}}$ with $\boldsymbol{G}$ standing for the reciprocal lattice vectors, and its corresponding eigenenergy is $\varepsilon_{n\boldsymbol{k}}$. In the plane wave basis, the wave function can also be expressed by the column vector $C_{n\boldsymbol{k}}$.

In calculating the optical conductivities, the velocity matrix elements $\boldsymbol{v}_{nm\boldsymbol{k}}$ between states $\psi_{n\boldsymbol{k}}$ and $\psi_{m\boldsymbol{k}}$ are necessary. A widely used method (A) is to approximate the velocity operator as $\hat{\boldsymbol{v}} = \hat{\boldsymbol{p}}/m_0$, with $\hat{\boldsymbol{p}}$ being the momentum operator; the matrix elements can be calculated immediately once the wave functions are obtained.[34,35] In this method, the contributions from the nonlocal part of the self-consistent potential and the spin-orbit coupling are only partially included. A more accurate method (B) is to extract the velocity matrix elements from ABINIT by performing response function calculations of the effect of a homogeneous electric field, at the cost of a large increase in computation time. These two methods are compared for the majority spin branch in $\sqrt{3}\times\sqrt{3}$ functionalized graphene: For the matrix elements between the impurity, the π, and the π^* bands, only minor differences are found; for other components, the difference can be large. However, the calculated optical conductivities are almost the same in the interesting photon energy range because the main contributions are from these three bands.

DFT calculations become very time-consuming for large supercells and dense $\boldsymbol{k}$-point grids. This makes it difficult to check the convergence of the optical conductivity, for which a grid finer than the one used in the ground state calculation is required. One systematic interpolation method based on the ground-state calculation uses the maximally localized Wannier functions.[36] Instead, for simplicity we use a direct interpolation method based on the $\boldsymbol{k}\cdot\boldsymbol{p}$ theory for which only $\psi_{n\boldsymbol{k}}$ and $\varepsilon_{n\boldsymbol{k}}$ obtained from ABINIT on a coarse grid are needed. Around $\boldsymbol{k}_0$, the Hamiltonian at $\boldsymbol{k}$ is written as

$$H_{\boldsymbol{k}} = U_{\boldsymbol{k}}\varepsilon_{\boldsymbol{k}}U_{\boldsymbol{k}}^{\dagger}, \tag{A1}$$

where $U_{\boldsymbol{k}}$ is a unitary matrix with elements $U_{mn\boldsymbol{k}} = \langle\psi_{m\boldsymbol{k}_0}|\psi_{n\boldsymbol{k}}\rangle = C^{\dagger}_{m\boldsymbol{k}_0}C_{n\boldsymbol{k}}$, and $\varepsilon_{\boldsymbol{k}}$ is a diagonal matrix for eigenenergies. Equation (A1) is exact taking into account the infinity number of bands. Considering only $\mathcal{N}$ bands, the unitarity of $U_{\boldsymbol{k}}$ is broken, but it can be recovered by approximating it as $\widetilde{U}_{\boldsymbol{k}} = T_{\boldsymbol{k}}Q_{\boldsymbol{k}}$, where $T_{\boldsymbol{k}}$ and $Q_{\boldsymbol{k}}$ are the left and right eigenvalues of $U_{\boldsymbol{k}} = T_{\boldsymbol{k}}\Sigma_{\boldsymbol{k}}Q_{\boldsymbol{k}}$ in the singular value decomposition. We then make the interpolation

$$\widetilde{H}_{\boldsymbol{k}} = H_0 + \sum_i V_i k_i + \frac{1}{2}\sum_{ij} M_{ij}k_ik_j, \tag{A2}$$

where H_0, V_i, and M_{ij} are $\mathcal{N}\times\mathcal{N}$ matrices. The fitting is performed taking points at the vertices and the edge midpoints of a triangle in reciprocal space with vertices $\{\boldsymbol{k}_i, i = 0,1,2\}$.

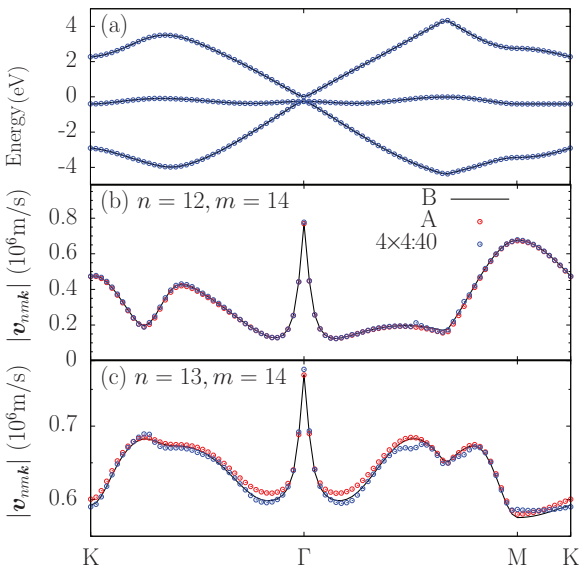

FIG. 9. (Color online) Comparison of the energy (a) and velocity matrix elements $|\boldsymbol{v}_{nm\boldsymbol{k}}|$ [(b), (c)] between the interpolated Hamiltonian and the results from ABINIT. The interpolation is for the majority branch of the $\sqrt{3}\times\sqrt{3}$ supercell on a 4×4 interpolation grid of 40 bands.

Corresponding to this Hamiltonian, the velocity operator is approximated as V_i. The comparisons between this interpolation, method A, and method B (taken as the exact result) are given in Fig. 9.

[1] A. H. Castro Neto, F. Guinea, N. M. R. Peres, K. S. Novoselov, and A. K. Geim, Rev. Mod. Phys. **81**, 109 (2009).

[2] D. S. L. Abergel, V. Apalkov, J. Berashevich, K. Ziegler, and T. Chakraborty, Adv. Phys. **59**, 261 (2010).

[3] F. Bonaccorso, Z. Sun, T. Hasan, and A. C. Ferrari, Nat. Photonics **4**, 611 (2010).

[4] R. R. Nair, P. Blake, A. N. Grigorenko, K. S. Novoselov, T. J. Booth, T. Stauber, N. M. R. Peres, and A. K. Geim, Science **320**, 1308 (2008).

[5] D. C. Elias, R. R. Nair, T. M. G. Mohiuddin, S. V. Morozov, P. Blake, M. P. Halsall, A. C. Ferrari, D. W. Boukhvalov, M. I. Katsnelson, A. K. Geim, and K. S. Novoselov, Science **323**, 610 (2009).

[6] H. Zhu, P. Huang, L. Jing, T. Zuo, Y. Zhao, and X. Gao, J. Mater. Chem. **22**, 2063 (2012).

[7] H. Zhang, E. Bekyarova, J.-W. Huang, Z. Zhao, W. Bao, F. Wang, R. C. Haddon, and C. N. Lau, Nano Lett. **11**, 4047 (2011).

[8] J. Hong, E. Bekyarova, P. Liang, W. A. de Heer, R. C. Haddon, and S. Khizroev, Sci. Rep. **2**, 624 (2012).

[9] R. Balog, B. Jorgensen, L. Nilsson, M. Andersen, E. Rienks, M. Bianchi, M. Fanetti, E. Laegsgaard, A. Baraldi, S. Lizzit, Z. Sljivancanin, F. Besenbacher, B. Hammer, T. G. Pedersen, P. Hofmann, and L. Hornekaer, Nat. Mater. **9**, 315 (2010).

[10] O. V. Yazyev, Rep. Prog. Phys. **73**, 056501 (2010).

[11] A. L. Ivanovskii, Russ. Chem. Rev. **81**, 571 (2012).

[12] W. Wei and X. Qu, Small **8**, 2138 (2012).

[13] D. W. Boukhvalov, M. I. Katsnelson, and A. I. Lichtenstein, Phys. Rev. B **77**, 035427 (2008).

[14] K. S. Choi and C. H. Park, J. Korean Phys. Soc. **54**, 939 (2009).

[15] J. Bang and K. J. Chang, Phys. Rev. B **81**, 193412 (2010).

[16] P. Chandrachud, B. S. Pujari, S. Haldar, B. Sanyal, and D. G. Kanhere, J. Phys. Condens. Matter **22**, 465502 (2010).

[17] A. R. Wright, T. E. O'Brien, D. Beaven, and C. Zhang, Appl. Phys. Lett. **97**, 043104 (2010).

[18] M. B. K. Milowska and J. Majewski, Acta Phys. Pol. A **120**, 842 (2011).

[19] A. I. Shkrebtii, E. Heritage, P. McNelles, J. L. Cabellos, and B. S. Mendoza, Phys. Status Solidi C **9**, 1378 (2012).

[20] E. J. Duplock, M. Scheffler, and P. J. D. Lindan, Phys. Rev. Lett. **92**, 225502 (2004).

[21] J. O. Sofo, A. S. Chaudhari, and G. D. Barber, Phys. Rev. B **75**, 153401 (2007).

[22] T. Miyake and S. Saito, Phys. Rev. B **72**, 073404 (2005).

[23] Z. Luo, J. Shang, S. Lim, D. Li, Q. Xiong, Z. Shen, J. Lin, and T. Yu, Appl. Phys. Lett. **97**, 233111 (2010).

[24] D. Haberer, L. Petaccia, Y. Wang, H. Quian, M. Farjam, S. A. Jafari, H. Sachdev, A. V. Federov, D. Usachov, D. V. Vyalikh, X. Liu, O. Vilkov, V. K. Adamchuk, S. Irle, M. Knupfer, B. Büchner, and A. Gürneis, Phys. Status Solidi B **248**, 2639 (2011).

[25] J. P. Robinson, H. Schomerus, L. Oroszlány, and V. I. Fal'ko, Phys. Rev. Lett. **101**, 196803 (2008).

[26] K. Pi, W. Han, K. M. McCreary, A. G. Swartz, Y. Li, and R. K. Kawakami, Phys. Rev. Lett. **104**, 187201 (2010).

[27] M. Gmitra, D. Kochan, and J. Fabian, Phys. Rev. Lett. **110**, 246602 (2013) .

[28] O. V. Yazyev and L. Helm, Phys. Rev. B **75**, 125408 (2007).

[29] O. V. Yazyev, Phys. Rev. Lett. **101**, 037203 (2008).

[30] X. Gonze, B. Amadon, P.-M. Anglade, J.-M. Beuken, F. Bottin, P. Boulanger, F. Bruneval, D. Caliste, R. Caracas, M. Côté, T. Deutsch, L. Genovese, P. Ghosez, M. Giantomassi, S. Goedecker, D. Hamann, P. Hermet, F. Jollet, G. Jomard, S. Leroux, M. Mancini, S. Mazevet, M. Oliveira, G. Onida, Y. Pouillon, T. Rangel, G.-M. Rignanese, D. Sangalli, R. Shaltaf, M. Torrent, M. Verstraete, G. Zerah, and J. Zwanziger, Comput. Phys. Commun. **180**, 2582 (2009); http://www.abinit.org.

[31] G. Weisz, Phys. Rev. **149**, 504 (1966).

[32] M. Gmitra, S. Konschuh, C. Ertler, C. Ambrosch-Draxl, and J. Fabian, Phys. Rev. B **80**, 235431 (2009).

[33] R. Nandkishore and L. Levitov, Phys. Rev. Lett. **107**, 097402 (2011).

[34] B. S. Mendoza, F. Nastos, N. Arzate, and J. E. Sipe, Phys. Rev. B **74**, 075318 (2006).

[35] F. Nastos, J. Rioux, M. Strimas-Mackey, B. S. Mendoza, and J. E. Sipe, Phys. Rev. B **76**, 205113 (2007).

[36] A. A. Mostofi, J. R. Yates, Y.-S. Lee, I. Souza, D. Vanderbilt, and N. Marzari, Comput. Phys. Commun. **178**, 685 (2008).